Improved Hydrogen Release from Ammonia Borane Confined in Microporous Carbon with Narrow Pore Size Distribution

Zhuxian Yang,[a] Dan Zhou,[b] Binling Chen,[a] Zongjian Liu,[c] Qinghua Xia,[b] Yanqiu Zhu,[a] and Yongde Xia[a,*]

[a] *College of Engineering, Mathematics and Physical Sciences, University of Exeter, Exeter EX4 4QF, United Kingdom. E-mail: y.xia@exeter.ac.uk*

[b] *Hubei Collaborative Innovation Centre for Advanced Organic Chemical Materials, & Ministry of Education Key Laboratory for the Synthesis and Application of Organic Functional Molecules, Hubei University, Wuhan 430062, China*

[c] *College of Chemical Engineering, Zhejiang University of Technology, Hangzhou 310014, China*

Abstract

Ammonia borane is a promising hydrogen storage candidate due to its high hydrogen capacity and good stability at room temperature, but there are still some barriers to be overcome before it can be used for practical applications. We present the hydrogen release from ammonia borane confined in templated microporous carbon with extremely narrow pore size distribution. Compared with neat ammonia borane, hydrogen release temperature of ammonia borane confined in microporous carbon with pore size of 1.05 nm is significantly reduced, starting at 50 °C and with peak dehydrogenation temperature centred at 86 °C. The dehydrogenation kinetics of ammonia borane confined in templated microporous carbon is significantly improved and by-products including ammonia and diborane are also completely prohibited without any catalysts involved. The remarkable fast hydrogen release rate and high hydrogen storage capacity from ammonia borane confined in microporous carbon is due to the dramatic decrease in the activation energy of ammonia borane. This is so far the best performance among porous carbon materials used as the confinement scaffolds for ammonia borane in hydrogen storage, making AB confined in microporous carbon a very promising candidate for hydrogen storage.

Introduction

The current widely used fossil fuels are non-renewable energy resources which will be depleted in the next century. Meanwhile, the use of fossil fuels inevitably emits greenhouse gas carbon dioxide into the air that has caused issues such as atmosphere pollution and global warming. Therefore, intensive efforts have been devoted to developing renewable energy resources that can replace fossil fuels in the near future. Hydrogen has been proposed as an ideal alternative energy resource since the burning of hydrogen only generates water, which is green and has no environmental concerns. One of the major issues for hydrogen as an energy vector is how to store this highly flammable gas effectively. Generally, four main methods to store hydrogen have been investigated so far including high pressure tanks, sorbents (such as porous carbons, metal-organic-frameworks), metal hydrides (such as $LiBH_4$ and $AlBH_4$) and chemical hydrides (such as ammonia borane). Each method has some advantages and drawbacks.[1, 2] Amongst these different hydrogen storage approaches, chemical hydrides are very promising and show higher gravimetric hydrogen capacities because they consist of lighter elements.

Ammonia borane (AB, $NH_3 \cdot BH_3$), a typical chemical hydride, has been intensively studied as a promising hydrogen storage media because of its high hydrogen capacities of 19.6 wt% and good stability at room temperature.[2, 3] AB dehydrogenates in three thermolysis steps at around 110, 150, and > 500 °C for the first, second, and third equivalents of H_2 respectively, with each step generating about 6.5 wt% hydrogen, which exceeds the revised target of hydrogen storage materials for light-duty vehicles as set by the US Department of Energy. Furthermore, recent reports have demonstrated that the spent fuel type derived from the removal of greater than two equivalents of H_2 per molecule of AB (i.e., polyborazylene) can be converted back to AB nearly quantitatively by 24-hour treatment with hydrazine in liquid ammonia at 40°C.[4, 5] However, despite these merits, there are technical barriers

preventing AB to be practically used as an on-board energy source, such as its slow thermal kinetics below 100 °C and unwanted by-products including ammonia (NH_3), diborane (B_2H_6), and borazine ($B_3H_6N_3$), which will poison the catalyst in a proton membrane fuel cell.[2, 3, 6-8]

To date, a number of ways have been investigated to tackle the above mentioned issues including the use of metal catalysts[3, 9-17] or metal-free catalysts,[18-20] the formation of metal hydrides,[21-23] the realisation of metal or methane substitution,[24-26] the utilisation of ionic liquid,[27, 28] additives,[29, 30] or nanoconfinement[8, 31-40] etc. Significant improvements on lowering the hydrogen release temperatures, improving the kinetics and avoiding the emissions of those harmful by-products have been made.

Confinement within porous materials has been reported to affect chemical reactions by modification of the thermodynamic properties due to adsorption, geometrical constraints in pores comparable to the molecular sizes, selective adsorption of reacting molecules, and changes of the potential energy surface, etc.[41] In particular, nano-confinement of hydrides into porous scaffold hosts has been reported to be able to alter the thermodynamics and kinetics of the hydrides significantly by reducing the dimension of hydride particles to nanoscale and therefore shorten the mass diffusion lengths; It is generally accepted that the confinement effect is inversely correlated to the average pore size of scaffold, i.e. the smaller the pore, the faster the kinetics.[42-44] The first report on nanoconfinement of AB in mesoporous silica demonstrated a lower dehydrogenation temperature, suppression of borazine release, and lower enthalpy of the decomposition,[31] which has triggered a number of studies in this area. Nanoscaffolds including mesoporous silica,[31, 45-47] mesoporous carbon,[32, 38, 48, 49] activated carbon,[50] carbon nanotubes,[39, 40] metal-organic frameworks (MOFs),[8, 33, 36, 37, 51-53] porous MnO_2[35] and low-density porous aromatic framework[34] have been studied. Particularly, MOFs have attracted much attention because of the combination of nanoporosity

and active metal sites in MOFs, which can offer a synergistic effect of nanoconfinement and metal site based catalysis.[8]

However, compared with porous carbon materials, MOFs and porous silicas are relatively heavy, which will inevitably compromise the hydrogen capacity of the nanocomposites. Yet only a couple of studies on porous carbon materials as the confinement hosts have been carried out so far.[32, 48-50] In particular, mesoporous carbon materials including coherent carbon cryogel[32, 48] and CMK-3[49] have been investigated. The coherent carbon cryogel/AB nanocomposite has exhibited lower dehydrogenation temperature and suppression of borazine;[32] and the mesoporous carbon CMK-3/AB nanocomposite has shown dehydrogenation in one-step at a significantly lower temperature but with the emission of ammonia, which can be avoided when a lithium catalyst is applied.[49] In addition, Sepehri et al have studied the effect of pore size on dehydrogenation temperature and kinetics of mesoporous coherent carbon/AB nanocomposites, showing that the smaller the pore, the better the dehydrogenation performance.[48] However, so far only mesoporous carbons with pore size in the range of 4.5 to 16 nm[32, 48, 49] have been investigated as scaffolds, and it is highly desirable and interesting to study the confinement effect when the pore of the carbon materials is further reduced down to micropore level (below 2 nm). Although recently activated carbons have been investigated as the scaffold, the composite dehydrogenates at room temperature causing safety issues (the composite is unstable).[50] Given that generally activated carbon exhibits a broad pore size distribution in the range of 0.3-2.0 nm,[54, 55] templated microporous carbon with narrow pore size distribution will be expected to perform better, which has not been explored in previous research.

In this regard, for the first time we report the hydrogen release from AB confined in microporous carbon with extremely narrow pore size distribution of 1.0 -1.5 nm, which was nanocasted using zeolite EMC-2 as the hard template. Without any catalysts involved,

hydrogen release temperature of AB from the nanocomposite is significantly reduced down to 50 °C with dehydrogenation peak centred at 86 °C. The dehydrogenation kinetics is improved and by-products including ammonia and diborane are prohibited in the nanocomposite system. The reason for the remarkable fast hydrogen release rate and high hydrogen storage capacity from ammonia borane confined in microporous carbon was addressed by comparing the activation energy of neat AB and AB confined microporous carbon.

Experimental Section

Sample preparation

Zeolite EMC-2 was synthesized following reported method.[56] The microporous carbon material was prepared via chemical vapor deposition (CVD) method using zeolite EMC-2 as the template and ethylene as the carbon precursor at 800 °C. In brief, 1 g of zeolite ECM-2 was put in a tube furnace under Ar flow, and when the temperature reached 800 °C, Ar flow was replaced by ethylene flow of 100 mL/m for 3 h, followed by cooling down under Ar flow. The resulting carbon/zeolite composite was washed with 10% hydrofluoric acid several times, followed by refluxing with concentrated hydrochloric acid at 60 °C to completely remove the zeolite framework. Finally, the resulting carbon material was dried in an oven at 120 °C overnight and named as CEMC. Thermogravimetric analysis (TGA) of the synthesized carbon was performed using a TA SDT Q600 instrument with a heating rate of 10 °C/min under an air flow of 100 mL/min, confirming the complete removal of the zeolite template. SEM-EDX also confirmed that only C and O were detected in the obtained carbon material.

AB was loaded into the microporous carbon CEMC by infusion of equivalent volume of AB-methanol solution to ECMC. Briefly, AB was dissolved in anhydrous methanol to form 1.0 M solution at room temperature, and the carbon was added into the calculated amount of methanol solution (based on the pore volume of ECMC) and stirred for several hours at room temperature. AB was incorporated into the pores of the carbon by the capillary effect. The solvent was removed via vacuum at room temperature overnight.

Sample characterisation

The X-ray diffraction (XRD) patterns were recorded using a Bruker D8 Advance diffractometer working with CuKα (Ni-filtered) radiation λ = 0.15418 nm and a scanning step size of $2\theta = 0.02^{o}$. The textural properties were determined via N_2 sorption at -196 °C on a Quantachrome Autosorb iQ sorptometer. The surface area was calculated using the Brunauer-Emmett-Teller (BET) method based on adsorption data in the partial pressure (P/P_0) range of 0.02-0.22 and the total pore volume was determined from the amount of nitrogen adsorbed at P/P_0 of *ca*. 0.99. The partial pressure range (P/P_0) 0.02 – 0.22 was selected for the calculation of surface area by taking into account previous report which indicates that low partial pressure range of P/P_0 0.01 – 0.05 will overestimate the surface area while the partial pressure range of P/P_0 0.1 – 0.3 can underestimate the surface area.[57] The pore size distribution (PSD) was obtained using the non-local density functional theory (NLDFT) method for slit/cylinder pores using the software provided by Quantachrome. The thermal gravimetric analysis (TGA) and decomposition process was carried out on a TA SDT Q600 instrument coupled with a mass spectrometer. The TGA was run with a heating ramp rate of 2 °C/min under argon flow of 100 mL/min, and the gaseous compositions from AB decomposition were determined by the coupled mass spectrometer. In the isotherm process, the sample was heated up to the target temperatures (70, 80 and 90 °C respectively) at a ramp rate of 20 °C/min under argon, then held at the isotherm temperature for 2 hours. Differential

scanning calorimetry (DSC) was determined with a Netszch DSC (204 HP Phoenix) at various ramp rates under argon flow. The amount of H_2 released from the sample was calculated based on the mass of AB in the material.

Results and discussion

The structure of neat AB, porous carbon CEMC, AB/CEMC before and after thermolysis at 200 °C was examined by XRD and shown in Fig. 1A. The XRD pattern of the carbon material CEMC shows two well resolved peaks at 2θ of 6.2^o and 6.8^o, which were at the same position as the (100) and (101) diffraction of the zeolite ECM-2. This observation clearly indicated that a high level of replication of zeolite-type structural ordering in the carbon material was realised, which is also in highly agreement with previous report results.[58-60] A further hump peak at 2θ of 26^o is due to the (002) diffraction line of partially graphitised carbon. The XRD pattern of AB/CEMC suggests that the loading of AB does not change the structure of the carbon CEMC. No XRD peaks of AB can be observed in AB/CEMC composite sample, implying that AB is indeed fully incorporated inside the pores rather than deposited on the outer surface of CECM matrix. The XRD pattern of AB/CEMC after thermolysis indicates that the structure of carbon CEMC does not change after the thermolysis of AB. Fig. 1B shows the nitrogen adsorption and desorption of CEMC and AB/CEMC, and the inset is the pore size distribution of CEMC. CEMC shows isotherm typical for microporous materials with surface area of 1652 $m^2 g^{-1}$ and pore volume of 0.87 $cm^3 g^{-1}$, and very narrow pore size distribution in the range of 1-1.5 nm, centred at 1.05 nm. It is worth noting that the pore size distributions of those mesoporous carbon materials reported as scaffolds are in a much broader range of 3-6 nm (for CMK-3[49, 61]), 3-20 nm (carbon cryogel[32]) and 5-20 nm (carbon cryogel[48]). However, the isotherm of the AB/CEMC

composite is almost a straight line with surface area of 56 $m^2 g^{-1}$ and pore volume of 0.04 $cm^3 g^{-1}$, implying that the pores of CEMC are almost completely occupied by the infiltrated AB, which is consistent with the XRD results.

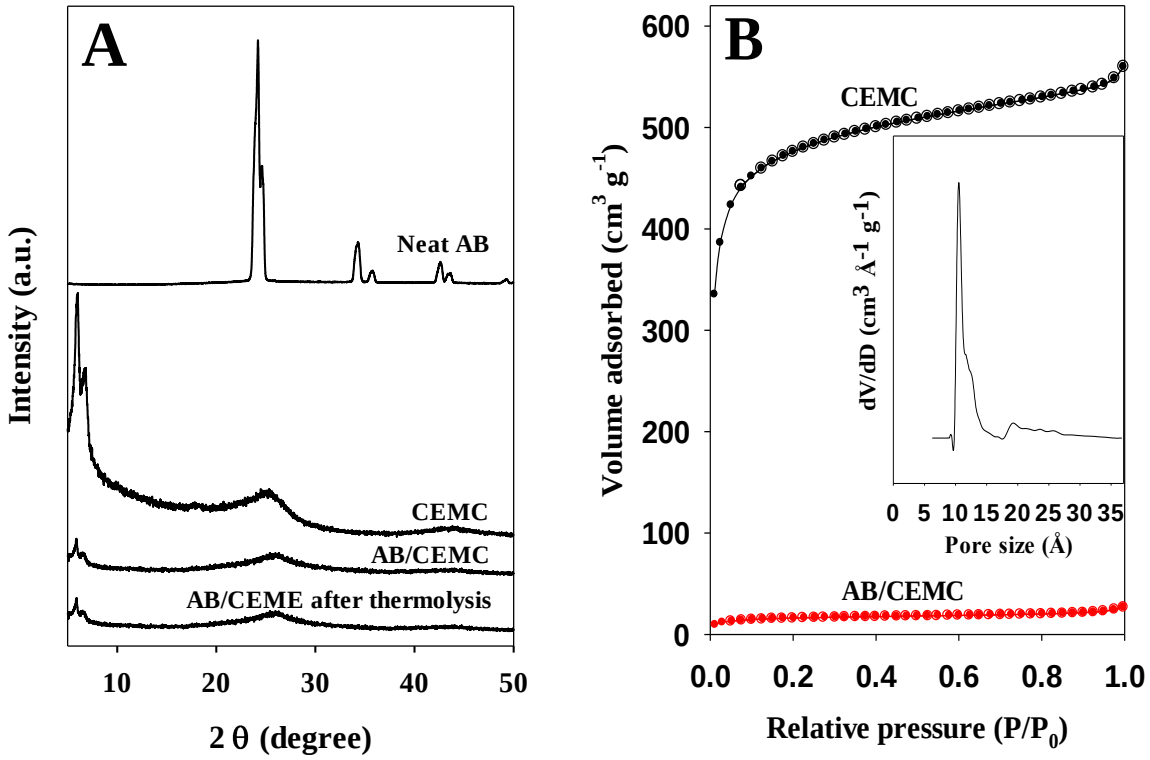

Fig. 1 Powder XRD patterns (A) of neat AB, porous carbon CEMC, and AB/CEMC before and after thermolysis at 200 °C, and N_2 adsorption (solid) and desorption (empty) isotherms (B) of neat CEMC (black) and AB/CEMC (red).

Fig. 2 presents the dehydrogenation profiles of AB and AB/CEMC obtained from thermogravimetric analysis (TGA) combined with mass spectroscopy (MS). Neat AB starts to dehydrogenate at above 100 °C via a two-step process and centres at 114 °C and 140°C respectively, with the emission of hydrogen, ammonia and diborane simultaneously, as evidenced by the MS signals, which is in good agreement with literature report.[8, 31] In the

case of AB/CEMC, dehydrogenation starts at much lower temperature of around 50 °C and peak dehydrogenation temperature is centred at 86 °C without any by-products detectable by MS. The absence of MS signals for by-products indirectly confirms that AB was totally deposited inside the pores of carbon scaffold rather than on the outside surface of the carbon. It has been demonstrated that when AB is fully located inside the pores of the scaffold, the formation of by-products is completely suppressed, whilst overloading of AB leads to partial AB deposited on the outside surface of carbon scaffold, which performs similar to bulk AB and results in the generation of by-products, due to the size effect.[62] Such a remarkable decrease of decomposition temperature for AB in CEMC is due to the effect of nano-confinement. It is worth pointing out that this is significant improvement compared to the mesoporous carbons as the scaffolds. For example, the peak dehydrogenation temperature of AB in mesoporous CMK-3 scaffold is 95 °C yet accompanied by the emission of ammonia and borazine; even when Li was introduced as the catalyst, the AB/Li-CMK-3 composite shows peak dehydrogenation temperature of 90 °C.[49] In addition, those coherent carbon cryogels as scaffolds results in peak dehydrogenation temperatures at 90, 98, 102 and 110 °C respectively.[32, 48] When activated carbon is used as the scaffold, the composite dehydrogenates at room temperature, causing safety issues.[50] Therefore this is the best result so far for porous carbon materials as the scaffold. It outperforms the poly(methyl acrylate) as scaffold too, which gives a peak temperature of 95 °C.[63] It is also better than[33] or comparable to those AB/MOF composites (84 °C).[8] We believe it is due to the small pore size and very narrow pore size distribution of the templated carbon CEMC, which enhances the confinement effect dramatically, in very good agreement with published results that smaller pores lead to better dehydrogenation performance.[48]

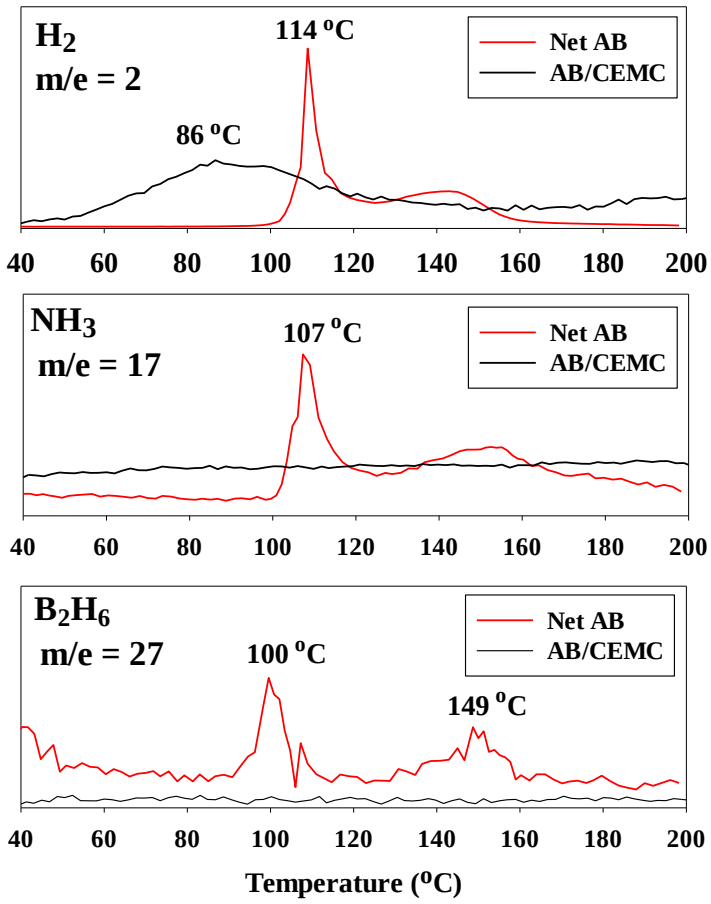

Fig. 2 The MS signals of H_2, NH_3 and B_2H_6 from neat AB and AB/CEMC composite between 40 and 200 °C at a heating rate of 2 °C/min in Ar.

The dehydrogenation rate of AB and AB/CEMC at various temperatures are shown in Fig. 3. AB/CEMC releases 7.6, 5.0 and 3.6 wt % hydrogen within 5 min at 90, 80 and 70 °C respectively, while neat AB does not release any hydrogen in the first 10 min regardless the temperatures under study, due to the long induction period for dehydrogenation of neat AB. Moreover, Around 9.9 and 7.0 wt% hydrogen released from AB confined in CEMC within 10 min at 90 and 80 °C respectively, which is much higher than the DOE bench mark hydrogen storage target of 5.5 wt% by 2015.[7] There have been no reported results on the dehydrogenation rate of AB confined in carbon materials but the dehydrogenation rate of AB

in CEMC is comparable to the results of AB confined in MOF JUC-32-Y.[8] The high hydrogen storage capacities combined with the fast hydrogen release rate of AB in CECM enables AB/CEMC promising for on-board applications. As shown in Fig 3B, after 40 min the hydrogen release of AB/CEMC at different isotherm temperature only shows slightly increase and at 70 °C the hydrogen release from AB/CEMC even remains unchanged, but at 90 °C the hydrogen release from AB/CEMC is gradually up to ~13.0 wt % within 2 h, which is the theoretical hydrogen for the first two-step dehydrogenation of AB.

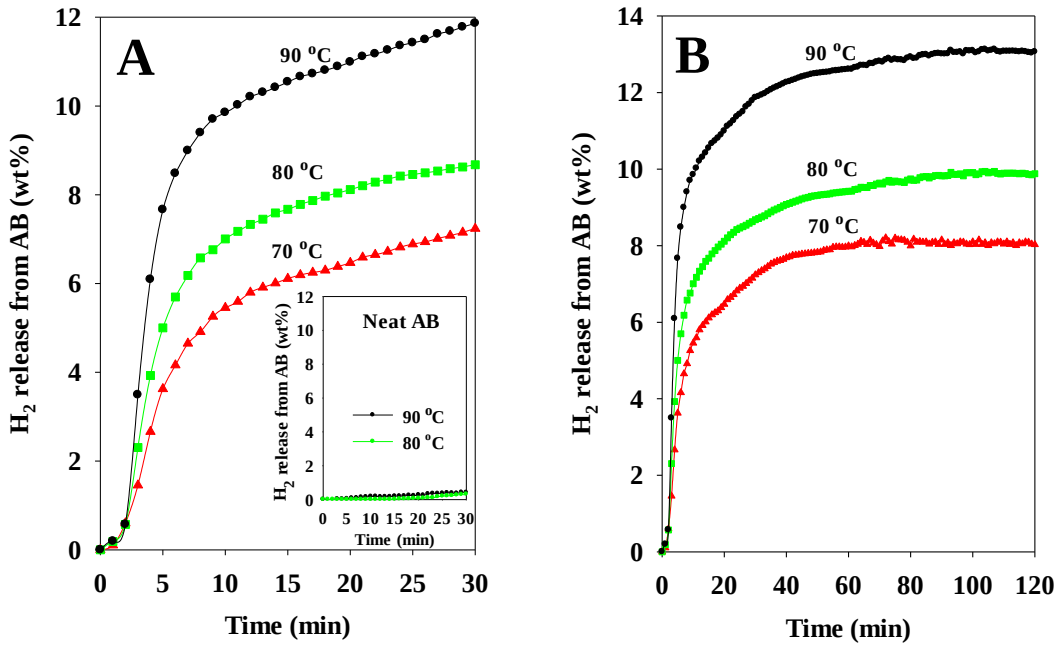

Fig. 3 Time dependence of hydrogen release of AB/CEMC at various temperatures for 30 min (A) or 2 h (B) respectively. The inset in left figure is the time dependence of hydrogen release of neat AB.

Due to the remarkable improvement in lowering the dehydrogenation temperature and fast dehydrogenation rate of AB confined in CEMC, we therefore evaluated the activation energy of the dehydrogenation for both neat AB and AB/CEMC to gain insight into the driving force

of the dramatic improvement. The activation energy was calculated by non-isothermal DSC runs under various heating rates, based on the Kissinger equation as follows:[64]

$$ln\frac{\beta}{T_{max}^2} = -\frac{E_a}{R}\left(\frac{1}{T_{max}}\right) + ln\frac{nAR(1-a_m)^{n-1}}{E_a} \qquad (1)$$

Where β is the heating rate; T_{max} is the maximum dehydrogenation temperature at different heating rates; E_a is the apparent dehydrogenation activation energy value; R is the universal gas constant and the A is a pre-exponential factor. The DSC profiles of neat AB at ramp rate of 2, 5, 10 15 °C/min and AB/CEMC at 2, 10 and 20 °C/min respectively are shown in Fig. S1 of ESI, and the Kissinger plots of AB and AB/CEMC derived from those DSC profiles are presented in Fig. 4. The activation energy of neat AB is about 131 kJ mol^{-1}, a little bit lower than reported values (180 kJ mol^{-1},[31] 160 kJ mol^{-1} [48]). The activation energy of AB/CEMC is about 75 kJ mol^{-1}, which is 56 kJ mol^{-1} lower than that of neat AB, indicating 43% decrease in activation energy. This is significant improvement compared to the AB/coherent carbon composites, which showed only 10 and 40 kJ mol^{-1} reduction respectively in the activation energy.[48] Due to the geometrical constraints of porous scaffold, the nano-confinement effect, as demonstrated in this work and the literature reports, can significantly lower the activation energy of the dehydrogenation of AB, which favours the breaking of B-H bond and N-H bond to produce H_2, but prevents the breaking of B-N bond, consequently supresses the formation of NH_3 and B_2H_6. In this work, the very narrow pore size distribution of the studied microporous carbon contributes to the remarkable decrease in activation energy of AB, therefore it accelerates the hydrogen release rate and depresses the emission of by-product including ammonia and diborane, consequently it results in high capacity of pure hydrogen release from the AB confined in CEMC.

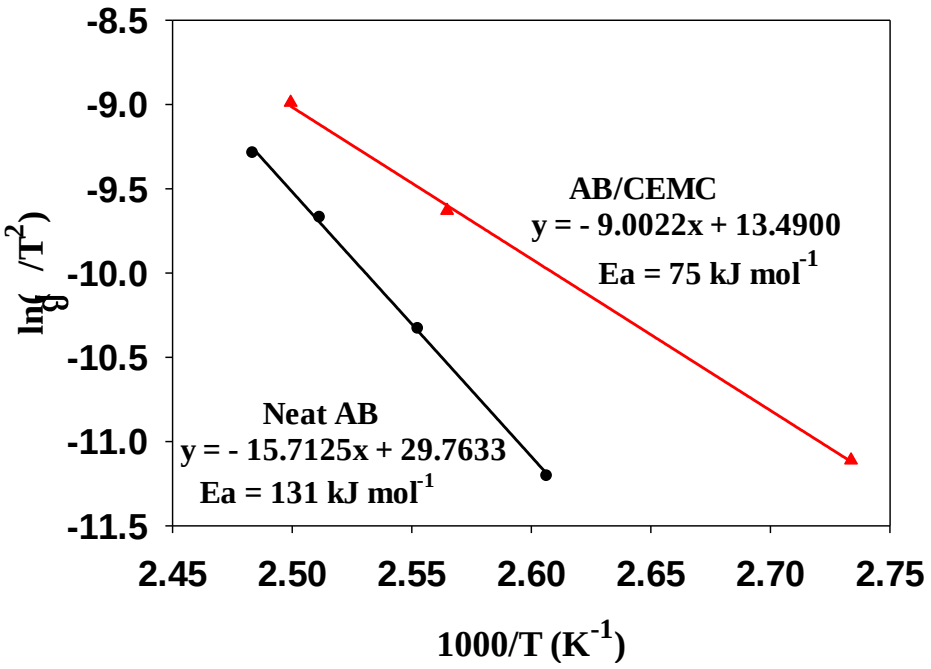

Fig. 4 Kissinger plots for net AB and AB/CEMC obtained from DSC with different heating rates.

Conclusions

This report has demonstrated that confining AB in microporous carbon with very narrow pore size distribution of 1-1.5 nm without any catalysts involved can significantly lower the hydrogen release temperature of AB from 114 ^{o}C down to 50°C with peak dehydrogenation temperature centred at 86 °C, remarkably improve the dehydrogenation kinetics and completely prohibit the emission of by-products including ammonia and diborane. This improvement is due to the dramatic decrease in the activation energy of AB confined in microporous carbon. This is the best performance to date for AB confined in porous carbon materials, making AB/CEMC a very promising candidate for hydrogen storage.

Acknowledgements

The financial support by the Royal Society and University of Exeter is greatly acknowledged.

Notes and References

1. H. W. Langmi and G. S. McGrady, *Coord. Chem. Rev.*, 2007, **251**, 925-935.
2. C. W. Hamilton, R. T. Baker, A. Staubitz and I. Manners, *Chem. Soc. Rev.*, 2009, **38**, 279-293.
3. N. C. Smythe and J. C. Gordon, *Eur. J. Inorg. Chem.*, 2010, DOI: 10.1002/ejic.200900932, 509-521.
4. B. L. Davis, D. A. Dixon, E. B. Garner, J. C. Gordon, M. H. Matus, B. Scott and F. H. Stephens, *Angew. Chem. Int. Ed.*, 2009, **48**, 6812-6816.
5. A. D. Sutton, A. K. Burrell, D. A. Dixon, E. B. Garner, J. C. Gordon, T. Nakagawa, K. C. Ott, P. Robinson and M. Vasiliu, *Science*, 2011, **331**, 1426-1429.
6. X. W. Chen, L. Wan, J. M. Huang, L. Z. Ouyang, M. Zhu, Z. P. Guo and X. B. Yu, *Carbon*, 2014, **68**, 462-472.
7. Supplement 1 to Original Targets for Onboard Hydrogen Storage Systems for Light-Duty Vehicles Published in September 2009 https://energy.gov/sites/prod/files/2015/05/f22/fcto_targets_onboard_hydro_storage_explanation.pdf.
8. Z. Li, G. Zhu, G. Lu, S. Qiu and X. Yao, *J. Am. Chem. Soc.*, 2010, **132**, 1490-1491.
9. C. A. Jaska, K. Temple, A. J. Lough and I. Manners, *J. Am. Chem. Soc.*, 2003, **125**, 9424-9434.

10. M. C. Denney, V. Pons, T. J. Hebden, D. M. Heinekey and K. I. Goldberg, *J. Am. Chem. Soc.*, 2006, **128**, 12048-12049.
11. R. J. Keaton, J. M. Blacquiere and R. T. Baker, *J. Am. Chem. Soc* 2007, **129**, 1844-1845.
12. A. Paul and C. B. Musgrave, *Angew. Chem. Int. Ed.*, 2007, **46**, 8153-8156.
13. N. Blaquiere, S. Diallo-Garcia, S. I. Gorelsky, D. A. Black and K. Fagnou, *J. Am. Chem. Soc.*, 2008, **130**, 14034-14035.
14. T. He, Z. Xiong, G. Wu, H. Chu, C. Wu, T. Zhang and P. Chen, *Chem. Mater.*, 2009, **21**, 2315-2318.
15. S.-K. Kim, W.-S. Han, T.-J. Kim, T.-Y. Kim, S. W. Nam, M. Mitoraj, L. Piekos, A. Michalak, S.-J. Hwang and S. O. Kang, *J. Am. Chem. Soc.*, 2010, **132**, 9954-9955.
16. K. Mori, K. Miyawaki and H. Yamashita, *ACS Catal.*, 2016, **6**, 3128-3135.
17. M. C. Wen, Y. W. Cui, Y. Kuwahara, K. Mori and H. Yamashita, *ACS Appl. Mater. Interface*, 2016, **8**, 21278-21284.
18. Z. P. Lu, L. Schweighauser, H. Hausmann and H. A. Wegner, *Angew. Chem. Int. Ed.*, 2015, **54**, 15556-15559.
19. D. W. Himmelberger, C. W. Yoon, M. E. Bluhm, P. J. Carroll and L. G. Sneddon, *J. Am. Chem. Soc.*, 2009, **131**, 14101-14110.
20. F. H. Stephens, R. T. Baker, M. H. Matus, D. J. Grant and D. A. Dixon, *Angew. Chem. Int. Ed.*, 2007, **46**, 746-749.
21. X. Kang, Z. Fang, L. Kong, H. Cheng, X. Yao, G. Lu and P. Wang, *Adv. Mater.*, 2008, **20**, 2756-2759.
22. J. H. Luo, X. D. Kang and P. Wang, *Int. J. Hydrogen Energy*, 2013, **38**, 4648-4653.
23. L. Wan, J. Chen, Y. B. Tan, Q. F. Gu and X. B. Yu, *Int. J. Hydrogen Energy*, 2015, **40**, 1047-1053.

24. Z. T. Xiong, C. K. Yong, G. T. Wu, P. Chen, W. Shaw, A. Karkamkar, T. Autrey, M. O. Jones, S. R. Johnson, P. P. Edwards and W. I. F. David, *Nat. Mater.*, 2008, **7**, 138-141.

25. H. V. K. Diyabalanage, R. P. Shrestha, T. A. Semelsberger, B. L. Scott, M. E. Bowden, B. L. Davis and A. K. Burrell, *Angew. Chem. Int. Ed.*, 2007, **46**, 8995-8997.

26. Y. S. Chen, J. L. Fulton, J. C. Linehan and T. Autrey, *J. Am. Chem. Soc.*, 2005, **127**, 3254-3255.

27. M. E. Bluhm, M. G. Bradley, R. Butterick, U. Kusari and L. G. Sneddon, *J. Am. Chem. Soc.*, 2006, **128**, 7748-7749.

28. W. R. H. Wright, E. R. Berkeley, L. R. Alden, R. T. Baker and L. G. Sneddon, *Chem. Commun.*, 2011, **47**, 3177-3179.

29. A. C. Gangal, R. Edla, K. Iyer, R. Biniwale, M. Vashistha and P. Sharma, *Int. J. Hydrogen Energy*, 2012, **37**, 3712-3718.

30. R. Q. Zhong, R. Q. Zou, T. Nakagawa, M. Janicke, T. A. Semelsberger, A. K. Burrell and R. E. Del Sesto, *Inorg. Chem.*, 2012, **51**, 2728-2730.

31. A. Gutowska, L. Y. Li, Y. S. Shin, C. M. M. Wang, X. H. S. Li, J. C. Linehan, R. S. Smith, B. D. Kay, B. Schmid, W. Shaw, M. Gutowski and T. Autrey, *Angew. Chem. Int. Ed.*, 2005, **44**, 3578-3582.

32. A. Feaver, S. Sepehri, P. Shamberger, A. Stowe, T. Autrey and G. Z. Cao, *J. Phys. Chem. B*, 2007, **111**, 7469-7472.

33. S. Gadipelli, J. Ford, W. Zhou, H. Wu, T. J. Udovic and T. Yildirim, *Chem. Eur. J.*, 2011, **17**, 6043-6047.

34. Y. Peng, T. Ben, D. J. Yang, H. J. Zhao, S. L. Qiu and X. D. Yao, *J. Phys. Chem. C*, 2012, **116**, 25694-25700.

35. Z. X. Yang, J. Liang, F. Y. Cheng, Z. L. Tao and J. Chen, *Microporous Mesoporous Mater.*, 2012, **161**, 40-47.

36. G. Srinivas, W. Travis, J. Ford, H. Wu, Z. X. Guo and T. Yildirim, *J. Mater. Chem. A*, 2013, **1**, 4167-4172.

37. H. M. Jeong, W. H. Shin, J. H. Park, J. H. Choi and J. K. Kang, *Nanoscale*, 2014, **6**, 6526-6530.

38. M. A. Wahab and J. N. Beltramini, *Int. J. Hydrogen Energy*, 2014, **39**, 18280-18290.

39. J. Alipour, A. M. Shoushtari and A. Kaflou, *J. Mater. Sci.*, 2015, **50**, 3110-3117.

40. L. J. Zhang, G. L. Xia, Y. Ge, C. Y. Wang, Z. P. Guo, X. G. Li and X. B. Yu, *J. Mater. Chem. A*, 2015, **3**, 20494-20499.

41. E. E. Santiso, A. M. George, C. H. Turner, M. K. Kostov, K. E. Gubbins, M. Buongiorno-Nardelli and M. Sliwinska-Bartkowiak, *Appl. Surf. Sci.*, 2005, **252**, 766-777.

42. A. F. Gross, J. J. Vajo, S. L. Van Atta and G. L. Olson, *J. Phys. Chem. C*, 2008, **112**, 5651-5657.

43. Z. Z. Fang, P. Wang, T. E. Rufford, X. D. Kang, G. Q. Lu and H. M. Cheng, *Acta Mater.*, 2008, **56**, 6257-6263.

44. Y. D. Xia, Z. X. Yang and Y. Q. Zhu, *J. Mater. Chem. A*, 2013, **1**, 9365-9381.

45. Y. Zhao, J. Zhang, D. L. Akins and J. W. Lee, *Ind. Eng. Chem. Res.*, 2011, **50**, 10024-10028.

46. T. Zhang, X. Yang, S. Yang, D. Li, F. Cheng, Z. Tao and J. Chen, *Phys. Chem. Chem. Phys.*, 2011, **13**, 18592-18599.

47. S. W. Lai, H. L. Lin, T. L. Yu, L. P. Lee and B. J. Weng, *Int. J. Hydrogen Energy*, 2012, **37**, 14393-14404.

48. S. Sepehri, B. B. Garcia and G. Z. Cao, *J. Mater. Chem. A*, 2008, **18**, 4034-4037.

49. L. Li, X. Yao, C. H. Sun, A. J. Du, L. N. Cheng, Z. H. Zhu, C. Z. Yu, J. Zou, S. C. Smith, P. Wang, H. M. Cheng, R. L. Frost and G. Q. M. Lu, *Adv. Func. Mater.*, 2009, **19**, 265-271.

50. G. Moussa, S. Bernard, U. B. Demirci, R. Chiriac and P. Miele, *Int. J. Hydrogen Energy*, 2012, **37**, 13437-13445.
51. X. l. Si, L. X. Sun, F. Xu, C. L. Jiao, F. Li, S. S. Liu, J. Zhang, L. F. Song, C. H. Jiang, S. Wang, Y. L. Liu and Y. Sawada, *Int. J. Hydrogen Energy*, 2011, **36**, 6698-6704.
52. Z. Y. Li, W. Liu, H. J. Yang, T. Sun, K. Liu, Z. H. Wang and C. Niu, *RSC Adv.*, 2015, **5**, 10746-10750.
53. H. J. Yang, Z. Y. Li, K. Liu, F. Y. Meng and C. Niu, *J. Phys. Chem. C*, 2015, **119**, 2260-2265.
54. E. A. Ustinov, D. D. Do and V. B. Fenelonov, *Carbon*, 2006, **44**, 653-663.
55. P. A. Gauden, A. P. Terzyk, G. Rychlicki, P. Kowalczyk, M. S. Cwiertnia and J. K. Garbacz, *J. Colloid Interface Sci.*, 2004, **273**, 39-63.
56. F. Delprato, L. Delmotte, J. L. Guth and L. Huve, *Zeolites*, 1990, **10**, 546-552.
57. K. Matsuoka, Y. Yamagishi, T. Yamazaki, N. Setoyama, A. Tomita and T. Kyotani, *Carbon*, 2005, **43**, 876-879.
58. Y. Xia, G. S. Walker, D. M. Grant and R. Mokaya, *J. Am. Chem. Soc.*, 2009, **131**, 16493-16499.
59. Y. Xia, R. Mokaya, D. M. Grant and G. S. Walker, *Carbon*, 2011, **49**, 844-853.
60. Y. Xia, Z. Yang, X. Gou and Y. Zhu, *Int. J. Hydrogen Energy*, 2013, **38**, 5039-5052.
61. S. Jun, S. H. Joo, R. Ryoo, M. Kruk, M. Jaroniec, Z. Liu, T. Ohsuna and O. Terasaki, *J. Am. Chem. Soc.*, 2000, **122**, 10712-10713.
62. G. Srinioas, J. Ford, W. Zhou and T. Yildirim, *Int. J. Hydrogen Energy*, 2012, **37**, 3633-3638.
63. J. Z. Zhao, J. F. Shi, X. W. Zhang, F. Y. Cheng, J. Liang, Z. L. Tao and J. Chen, *Adv. Mater.*, 2010, **22**, 394-397.
64. H. E. Kissinger, *Anal. Chem.*, 1957, **29**, 1702-1706.